50. Oligosaccharides Related to Tumor-Associate Antigens

Part 4[1])

Modeling of the Terminal Tetrasaccharide of an Antigen Recognized by the MBr1 Antibody and of Overlapping Di- and Trisaccharide Sequences

by **Lucio Toma***

Dipartimento di Chimica Organica, Università di Pavia, Via Taramelli 10, I–27100 Pavia

and **Diego Colombo** and **Fiamma Ronchetti**

Dipartimento di Chimica e Biochimica Medica, Università di Milano, Via Saldini 50, I–20133 Milano

and **Luigi Panza** and **Giovanni Russo**

Dipartimento di Chimica Organica e Industriale, Università di Milano, Via Venezian 21, I–20133 Milano

(23.I.95)

The conformational space of the tetrasaccharide α-L-Fuc-(1→2)-β-D-Gal-(1→3)-β-D-GalNAc-(1→3)-α-D-Gal1Pr (**3**) and of some overlapping di- and trisaccharide sequences was investigated with the aid of molecular-mechanics energy minimizations, molecular-dynamics simulations, and ^{1}H-NMR analysis. These investigations suggested that in compound **3** a certain rigidity of the first two glycosidic linkages (Fuc-Gal and Gal-GalNAc) is combined with the flexibility of the third one (GalNAc-Gal).

Introduction. – In previous papers [2] [3], we described the synthesis and the modeling of the trisaccharide α-L-Fuc-(1→2)-β-D-Gal-(1→3)-β-D-GalNAc1Pr (**1**), the *a-b-c* component of the glycolipid antigen globo-H α-L-Fuc-(1→2)-β-D-Gal-(1→3)-β-D-GalNAc-(1→3)-α-D-Gal-(1→4)-β-D-Gal-(1→4)-β-D-Glc-(1→1)-Cer (**2**), overexpressed by breast-cancer cells and recognized by the antibody MBr1 [4].

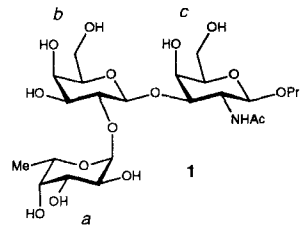

1

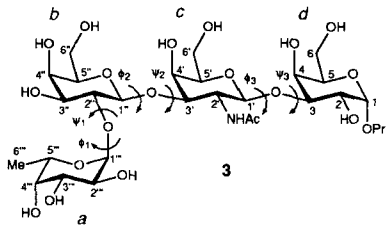

3

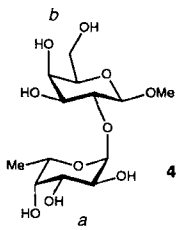

4

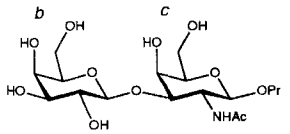

5

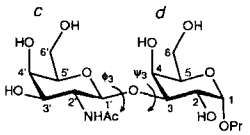

6

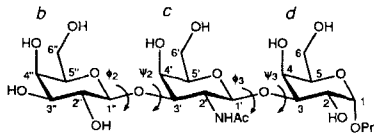

7

[1]) Part 3: [1].

Trisaccharide **1** is the nonreducing terminus of the hexasaccharide which represents the glycoside portion of **2**. It was chosen as the object of the first studies as it was supposed to be the epitope recognized by the antibody MBr1. However, when the *a-b-c-d* tetrasaccharide α-L-Fuc-(1→2)-β-D-Gal-(1→3)-β-D-GalNAc-(1→3)-α-D-Gal1Pr (**3**) was synthesized and its affinity for the MBr1 antibody evaluated [1], the antigen-antibody recognition resulted enforced sevenfold with respect to the MBr1-trisaccharide **1** interaction. To determine the influence of the α-D-Gal residue *d* on the conformational behavior of the saccharide as such and its possible role in the interaction with the antibody, we submitted the tetrasaccharide **3** to molecular modeling. Theoretical and spectroscopical approaches were used to ascertain its conformational properties and were applied not only to **3** but also, in a stepwise approach, to overlapping di- and trisaccharide sequences.

Results and Discussion. – The same approach already used for the modeling of the *a-b-c* trisaccharide **1** was used for the *a-b-c-d* tetrasaccharide **3**: the component di- and trisaccharides were considered before studying the entire **3**. There are three component disaccharide moieties: *a-b* (**4**), *b-c* (**5**), and *c-d* (**6**); only the third required to be studied as α-L-Fuc-(1→2)-β-D-Gal1Me (**4**) and β-D-Gal-(1→3)-β-D-GalNAc1Pr (**5**) were already modeled in [3]. For the same reasons, of the two component trisaccharide moieties *a-b-c* (**1**) and *b-c-d* (**7**), only the latter required to be studied. Thus, the theoretical calculations and the spectroscopic investigations for the disaccharide **6**, the trisaccharide **7**, and the tetrasaccharide **3**, all considered as propyl glycosides, are reported here.

The conformational space of disaccharide **6** was investigated with a molecular-mechanics approach followed by molecular-dynamics simulations. Thirty-six starting ge-

Table 1. *Data on the Minimum-Energy Conformations of Disaccharide* **6**, *Trisaccharide* **7**, *and Tetrasaccharide* **3** *as Calculated by Molecular Mechanics*

	Conformation	ϕ_1, ψ_1 [°]	ϕ_2, ψ_2 [°]	ϕ_3, ψ_3 [°]	E_{rel} [kcal/mol]	Equilibrium percentage
6	**6B**			16, −52	0.00	89.0
	6A			28, 33	1.37	8.8
	6C			63, 65	2.22	2.1
	6D			22, 165	3.88	0.1
7	**7AB**		36, 25	22, −55	0.00	44.5
	7BB		29, −53	16, −52	0.40	22.6
	7CB		69, 67	14, −53	0.47	20.1
	7AA		38, 23	32, 34	1.12	6.7
	7BA		38, −39	30, 34	1.86	1.9
	7AC		36, 25	63, 65	1.93	1.7
	7CA		68, 68	28, 40	2.26	1.0
	7BC		38, −38	64, 64	2.69	0.5
	7CC		68, 67	57, 63	2.85	0.4
3	**3BBB**	22, −54	29, −51	16, −52	0.00	71.2
	3AAB	34, 26	40, 24	16, −52	0.79	18.7
	3BBA	21, −52	27, −51	20, 40	1.68	4.2
	3BCB	24, −57	66, 71	17, −53	1.70	4.0
	3AAA	34, 26	40, 23	25, 38	2.63	0.8
	3ACB	31, 29	69, 68	15, −53	2.72	0.7
	3BCA	24, −56	66, 71	27, 38	3.56	0.2
	3BBC	21, −54	29, −51	59, 64	3.65	0.2

ometries were prepared by rigid rotation around the glycosidic bonds ϕ and ψ covering the entire ϕ/ψ map with a 60° grid. These starting geometries were fully relaxed by using the HyperChem MM$^+$ force field to yield several minima for which the orientations of the CH_2OH and OH groups were optimized. *Table 1* reports the data of the conformers found in a range of 4 kcal/mol above the global minimum, and *Fig. 1* shows the 3D plots of the most populated conformations.

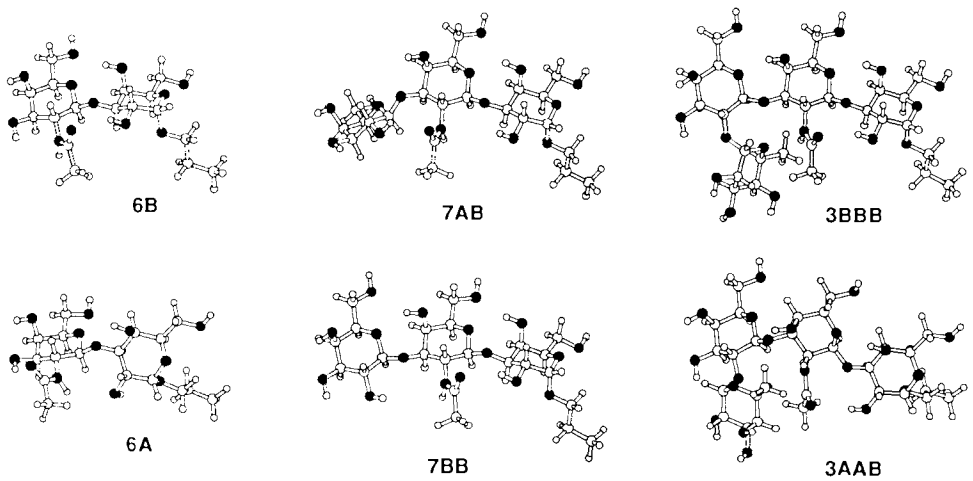

Fig. 1. *Three-dimensional plots of the most populated conformers of disaccharide* **6**, *trisaccharide* **7**, *and tetrasaccharide* **3**

The behavior of the disaccharide **6** is very similar to that of the previously studied disaccharides **4** and **5**. Once again, two minima are practically sufficient to describe the conformational distribution as they account for *ca.* 98% of the overall population. The global minimum **6B** at $\phi_3 = 16°$ and $\psi_3 = -52°$ corresponds to the global minimum of **4**, and the next minimum **6A** at $\phi_3 = 28°$ and $\psi_3 = 33°$ corresponds to the global minimum of **5**. The third minimum **6C** ($\phi_3 = 63°$, $\psi_3 = 65°$) is very close to **6A** and is separated from it by a very low energy barrier; it contributes for *ca.* 2% to the overall population[2]).

Molecular-dynamics (MD) simulations of compound **6** were also performed starting from the four minima **3A–D**, consisting in a pre-equilibration period (20 ps) followed by 80 ps data-collection periods. In *Fig. 2* are reported the trajectories of the ϕ_3 and ψ_3 angles *vs.* time and in *Fig. 3* the ϕ_3 *vs.* ψ_3 trajectories. The energy barrier between the **6A** and **6B** conformers is very low. A high number of **A** → **B** and **B** → **A** transitions can be observed in all four simulations indicating that minima **6A** and **6B** represent for the disaccharide **6** two conformers of a unique low-energy region. The simulation from **6C** results in a transition to the **A**/**B** region after a few ps, some back transition is observed, but the **C** region is less populated than the **A** and **B** regions. The simulation from **6D** shows a transition to the more stable regions after 50 ps with observation of no back transition.

---

[2]) In all saccharides under study, we used **A** to denote an energy minimum on the ϕ/ψ map located at ϕ values of 20–40° and ψ values of 20–40°, **B** to denote a minimum located at ϕ values of 10–40° and ψ values of −40 to −60°, and **C** to denote a minimum located at ϕ values of 60°–70° and ψ values of 60–70°.

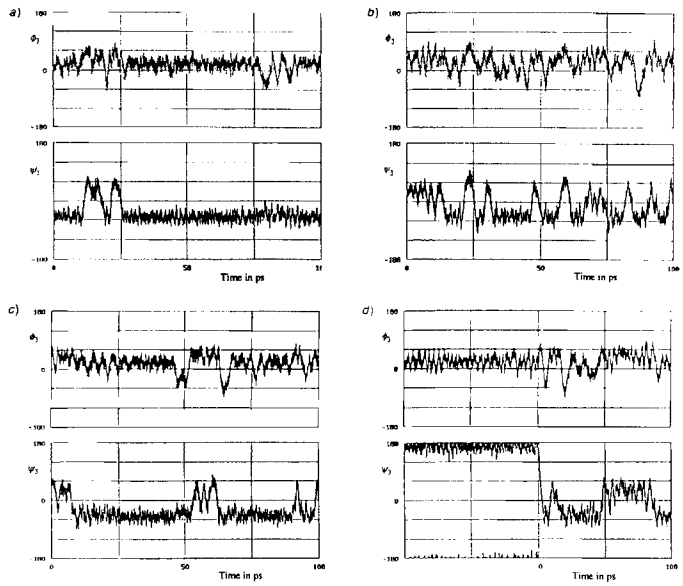

Fig. 2. *History of ϕ_3 and ψ_3 for the MD simulations starting from* a) **6A**, b) **6B**, c) **6C**, *and* d) **6D** *over the entire trajectory, including equilibration*

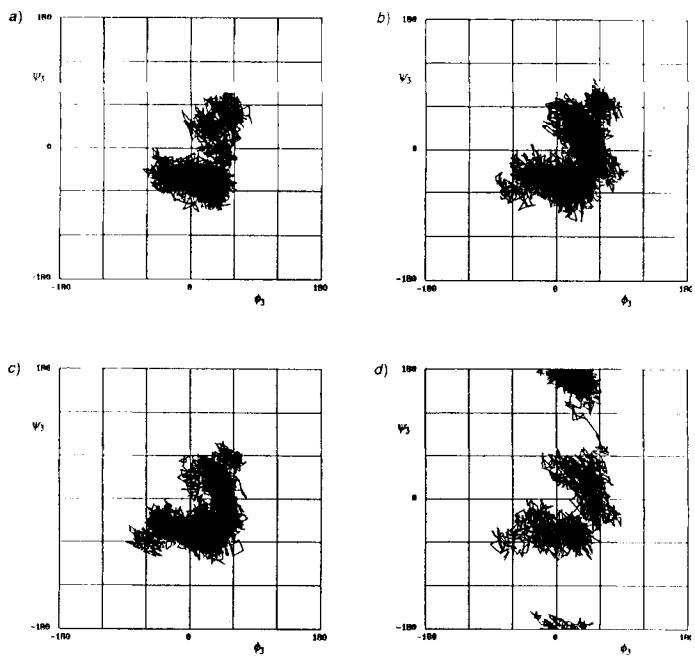

Fig. 3. *Trajectories on the ϕ_3/ψ_3 map for the MD simulations starting from* a) **6A**, b) **6B**, c) **6C**, *and* d) **6D**, *including equilibration*

The energy barrier which protects conformer **6D**, though higher than that protecting conformer **6C**, can be easily passed after a few tenths of ps.

As a result of the static (*Table 1*) and the dynamic (*Figs. 2* and *3*) representations of compound **6**, a contribution of both the **6A** and **6B** conformers is predicted by the calculations, though the determination of the true balance between them requires the aid of experimental data. Complete assignment of the ^{1}H-NMR spectrum of disaccharide **6** is a prerequisite to gaining insight into its conformations in aqueous solution. The ^{1}H-NMR resonances were assigned by standard methods that rely on correlation through chemical bonds or through space and are reported in *Table 2*, while *Table 3* reports the inter-residue contacts obtained from ROESY experiments. Moreover, in the same *Table 3* are reported the corresponding distances either calculated for the different energy minima of **6** or averaged from the MD simulations as $r = [\langle r^{-3} \rangle]^{-1/3}$ taking into account the nonlinear distance dependence of the NOE effect [5].

Table 2. *^{1}H-NMR Spectral Data* (D_2O, 500 MHz) *for Compounds* **2–4**. δ(H) values in ppm referenced to HDO at δ 4.55, J in Hz.

	Disaccharide **6**		Trisaccharide 7		Tetrasaccharide **3**	
	H-Atom	δ (J)	H-Atom	δ (J)	H-Atom	δ (J)
Residue *a*					H–C(1‴)	5.05 (J(1‴,2‴) = 4.0)
α-L-Fuc					H–C(2‴)	3.59 (J(2‴,3‴) = 10.0)
					H–C(3‴)	3.47 (J(3‴,4‴) = 3.5)
					H–C(4‴)	3.54 (J(4‴,5‴) ≤ 1)
					H–C(5‴)	4.06 (J(5‴,6‴) = 6.5)
					H–C(6‴)	1.04
Residue *b*			H–C(1″)	4.26 (J(1″,2″) = 7.5)	H–C(1″)	4.44 (J(1″,2″) = 7.5)
β-D-Gal			H–C(2″)	3.35 (J(2″,3″) = 10.0)	H–C(2″)	3.45 (J(2″,3″) = 10.0)
			H–C(3″)	3.43 (J(3″,4″) = 3.5)	H–C(3″)	3.65 (J(3″,4″) = 3.5)
			H–C(4″)	3.73 (J(4″,5″) ≤ 1)	H–C(4″)	3.72 (J(4″,5″) ≤ 1)
			H–C(5″)	3.46 (J(5″,6″$_a$) = 4.5)	H–C(5″)	3.48 (J(5″,6″$_a$) = 4.5)
			2H–C(6″)	3.54–3.60 (J(5″,6″$_b$) = 7.5)	2H–C(6″)	3.55–3.63 (J(5″,6″$_b$) = 7.5)
Residue *c*	H–C(1′)	4.46 (J(1′,2′) = 8.5)	H–C(1′)	4.52 (J(1′,2′) = 8.5)	H–C(1′)	4.37 (J(1′,2′) = 7.5)
β-D-GalNAc	H–C(2′)	3.75 (J(2′,3′) = 10.5)	H–C(2′)	3.86 (J(2′,3′) = 10.5)	H–C(2′)	3.82 (J(2′,3′) = 10.5)
	H–C(3′)	3.56 (J(3′,4′) = 3.5)	H–C(3′)	3.72 (J(3′,4′) = 3.0)	H–C(3′)	3.78 (J(3′,4′) = 2.5)
	H–C(4′)	3.76 (J(4′,5′) ≤ 1)	H–C(4′)	3.99 (J(4′,5′) ≤ 1)	H–C(4′)	3.93 (J(4′,5′) ≤ 1)
	H–C(5′)	3.48 (J(5′,6′$_a$) = 4.5)	H–C(5′)	3.50 (J(5′,6′$_a$) = 4.5)	H–C(5′)	3.52 (J(5′,6′$_a$) = 4.5)
	H$_a$–C(6′)	3.61 (J(5′,6′$_b$) = 7.5)	2H–C(6′)	3.54–3.60 (J(5′,6′$_b$) = 7.5)	2H–C(6′)	3.55–3.63 (J(5′,6′$_b$) = 7.5)
	H$_b$–C(6′)	3.57 (J(6′$_a$,6′$_b$) = 11.5)				
Residue *d*	H–C(1)	4.73 (J(1,2) = 3.5)	H–C(1)	4.73 (J(1,2) = 3.5)	H–C(1)	4.71 (J(1,2) = 3.7)
α-D-Gal	H–C(2)	3.69 (J(2,3) = 10.0)	H–C(2)	3.69 (J(2,3) = 10.5)	H–C(2)	3.65 (J(2,3) = 10.0)
	H–C(3)	3.74 (J(3,4) = 3.0)	H–C(3)	3.74 (J(3,4) = 3.0)	H–C(3)	3.73 (J(3,4) = 3.5)
	H–C(4)	4.01 (J(4,5) ≤ 1)	H–C(4)	4.00 (J(4,5) ≤ 1)	H–C(4)	4.01 (J(4,5) ≤ 1)
	H–C(5)	3.78 (J(5,6) = 6.5)	H–C(5)	3.76 (J(5,6) = 6.0)	H–C(5)	3.78 (J(5,6) = 6.0)
	2H–C(6)	3.54	2H–C(6)	3.54	2H–C(6)	3.54
	CH_aO	3.31 (J(H_a,H_b) = 9.5)	CH_aO	3.31 (J(H_a,H_b) = 9.5)	CH_aO	3.31 (J(H_a,H_b) = 9.5)
	CH_bO	3.48 (J(H_a,CH_2) = 6.5)	CH_bO	3.47 (J(H_a,CH_2) = 6.5)	CH_bO	3.48 (J(H_a,CH_2) = 6.2)
	CH_2	1.45 (J(H_b,CH_2) = 7.0)	CH_2	1.44 (J(H_b,CH_2) = 7.0)	CH_2	1.45 (J(H_b,CH_2) = 7.0)
	Me	0.74 (J(CH_2,Me) = 7.5)	Me	0.74 (J(CH_2,Me) = 7.5)	Me	0.75 (J(CH_2,Me) = 7.5)
	Ac	1.86	Ac	1.85	Ac	1.86

Table 3. *Inter-Residue Contacts Derived from the Phase-Sensitive ROESY Experiments and Corresponding Distances* [Å] *from MM and MD Calculations*

		ROESY cross-peaks[a])	Calc. distance for the minimum-energy conformations				Calc. distance in the MD simulations	
			6A	**6B**	**6C**	**6D**	from **6A**	from **6B**
6	H–C(1′)/H–C(3)	s	2.35	2.26	3.19	3.60	2.35	2.29
	H–C(1′)/H–C(4)	w	4.29	2.53	4.61	3.50	2.86	2.57

		ROESY cross-peaks[a])	Calc. distance for the minimum-energy conformations							Calc. distance in the MD simulation
			7AB	**7BB**	**7CB**	**7AA**	**7BA**	**7AC**	**7CA**	from **7AB**
7	H–C(1″)/H–C(3′)	s	2.35	2.26	3.27	2.35	2.21	2.35	3.27	2.32
	H–C(1″)/H–C(4′)	w	4.27	2.70	4.62	4.25	3.21	4.26	4.62	3.05
	H–C(1′)/H–C(3)	s	2.28	2.26	2.26	2.41	2.38	3.18	2.44	2.33
	H–C(1′)/H–C(4)	w	2.51	2.53	2.48	4.33	4.31	4.62	4.36	2.89

		ROESY cross-peaks[a])	Calc. distance for the minimum-energy conformations					Calc. distance in the MD simulations	
			3AAB	**3BCB**	**3AAA**	**3BBB**	**3BBA**	from **3AAB**	from **3BBA**
3	H–C(1‴)/H–C(2″)	s	2.34	2.30	2.32	2.27	2.26	2.44	2.29
	H–C(1‴)/H–C(3″)	w	3.62	4.45	3.62	4.45	4.46	3.61	4.40
	H–C(1″)/H–C(3′)	s	2.37	3.30	2.37	2.25	2.24	2.42	2.29
	H–C(1″)/H–C(4′)	w	4.27	4.61	4.27	2.77	2.75	4.02	2.65
	H–C(1′)/H–C(3)	s	2.26	2.26	2.39	2.26	2.41	2.30	2.34
	H–C(1′)/H–C(4)	w	2.51	2.52	4.32	2.52	4.34	2.65	3.03
	H–C(5‴)/H–C(1″)	w	3.46	2.84	3.45	2.94	2.97	3.67	3.12
	H–C(5‴)/H–C(2′)	s	2.38	3.96	2.40	5.96	5.95	2.82	6.23
	CH_3(6‴)/H–C(2′)	w	3.26	2.85	3.25	5.46	5.44	3.82	5.93
	H–C(3‴)/Ac	w	3.05	8.36	3.08	5.90	5.90	3.58	6.19
	H–C(1″)/Ac	w	4.00	4.09	4.03	6.38	6.40	4.09	6.36

[a]) s: strong; w: weak.

Besides the high interaction H–C(1′)/H–C(3), the low interaction of H–C(1′) with H–C(4) was detected. The distances obtained from the MD simulations are to be compared with these contacts; the dynamic equilibria of conformers **6A** and **6B** give rise to H–C(1′)/H–C(3) distances (2.35 or 2.29 Å) which well account for a strong ROESY cross-peak; the predicted H–C(1′)/H–C(4) distance (2.86 or 2.57 Å) is perhaps too short for a low ROESY cross-peak indicating that the contribution of conformer **6A** with respect to **6B** is actually higher than that expressed by the calculations. So, while the theoretical predictions favor the **6B** conformer, the results of the NMR analysis indicate that the molecule spends most of the time in the **A** region. This result closely parallels the behavior of the disaccharides **4** and **5**.

The exploration of the conformational space of the trisaccharide **7** and of the tetrasaccharide **3** through molecular-mechanics optimizations was limited to the regions allowed for the component disaccharides: so, we chose as starting geometries of **7** and **3** all conformations showing glycosidic-bond dihedral angles corresponding to the values

found as minima for the component disaccharides. After minimization and optimization of the orientation of the CH_2OH and OH groups, several minima were found for the two oligosaccharides. *Table 1* summarizes the data of the conformers found in a range of 3 kcal/mol above the global minimum, and *Fig. 1* shows the 3D plots of the most populated conformers.

Also in these cases, we performed MD simulations at 300 K starting from the optimized conformers. In *Figs. 4* and *5* are reported the trajectories of the simulation

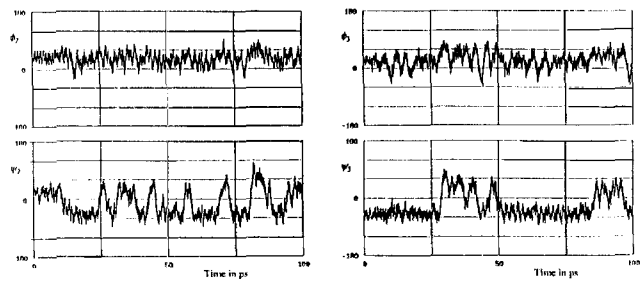

Fig. 4. *History of ϕ_2, ψ_2, ϕ_3, and ψ_3 for the MD simulations starting from* **7AB** *over the entire trajectory, including equilibration*

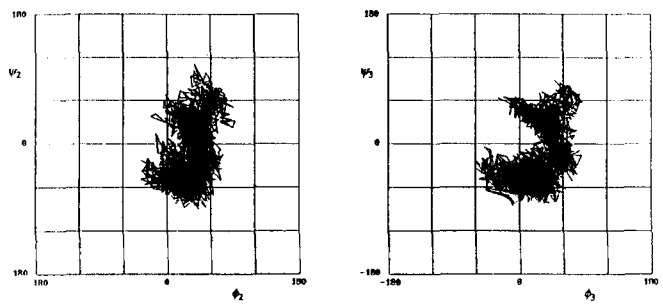

Fig. 5. *Trajectories on the ϕ_2/ψ_2 and ϕ_3/ψ_3 maps for the MD simulations starting from* **7AB**, *including equilibration*

starting from conformer **7AB**. As it can be seen either from the trajectories of ϕ and ψ *vs.* time or in the ϕ *vs.* ψ trajectories the molecule can easily visit all conformers found as minima and reported in *Table 1*. The energy barriers separating the **A**, **B**, (and **C**) regions are so low that several transitions among them are possible. This behaviour, compared with that of disaccharides **5** and **6**, in which easy transitions were observed between the conformers of type **A** and **B**, indicates that in **7** there is no influence of one glycosidic linkage on the other; this fact is also confirmed by the shapes of the ϕ_2 *vs.* ψ_2 and ϕ_3 *vs.* ψ_3 trajectories of **7** which are very similar to the corresponding ϕ_2/ψ_2 trajectories of **5** [3] and ϕ_3/ψ_3 trajectories of **6**.

The ROESY results for **7** (*Table 3*) closely parallel the results of the theoretical calculations as they show high cross-peaks for the H–C(1″)/H–C(3′) and H–C(1′)/H–C(3) interactions where the averaged calculated distances are 2.32 and 2.33 Å, respec-

tively, and two low cross-peaks for the H–C(1″)/H–C(4′) and H–C(1′)/H–C(4) interactions where the averaged calculated distances are 2.89 and 3.05 Å, respectively.

The conformational flexibility found for **7** contrasts with the rigidity of the trisaccharide **1** [3] where each glycosidic linkage heavily limits the mobility of the other owing to the presence of the fucose residue *a*.

In *Figs. 6* and *7* three different MD simulations on the tetrasaccharide **3** are reported. The simulation starting from **3AAB** shows that no transition from the **A** to the **B** region is observed at the Fuc-Gal (*a-b*) glycosidic linkage. The Gal-GalNAc (*b-c*) glycosidic linkage is slightly more flexible but the negative values of the ψ_2 trajectory in *Fig. 6a* actually do not represent true transitions from the **A** to the **B** region; in fact extraction of some of these conformations followed by energy minimization lead to optimized structures of the **AAB** type. This fact means that when the *a-b* glycosidic linkage assumes a conformation of the **A** type, there is no minimum of the *b-c* linkage in the **B** region. On the

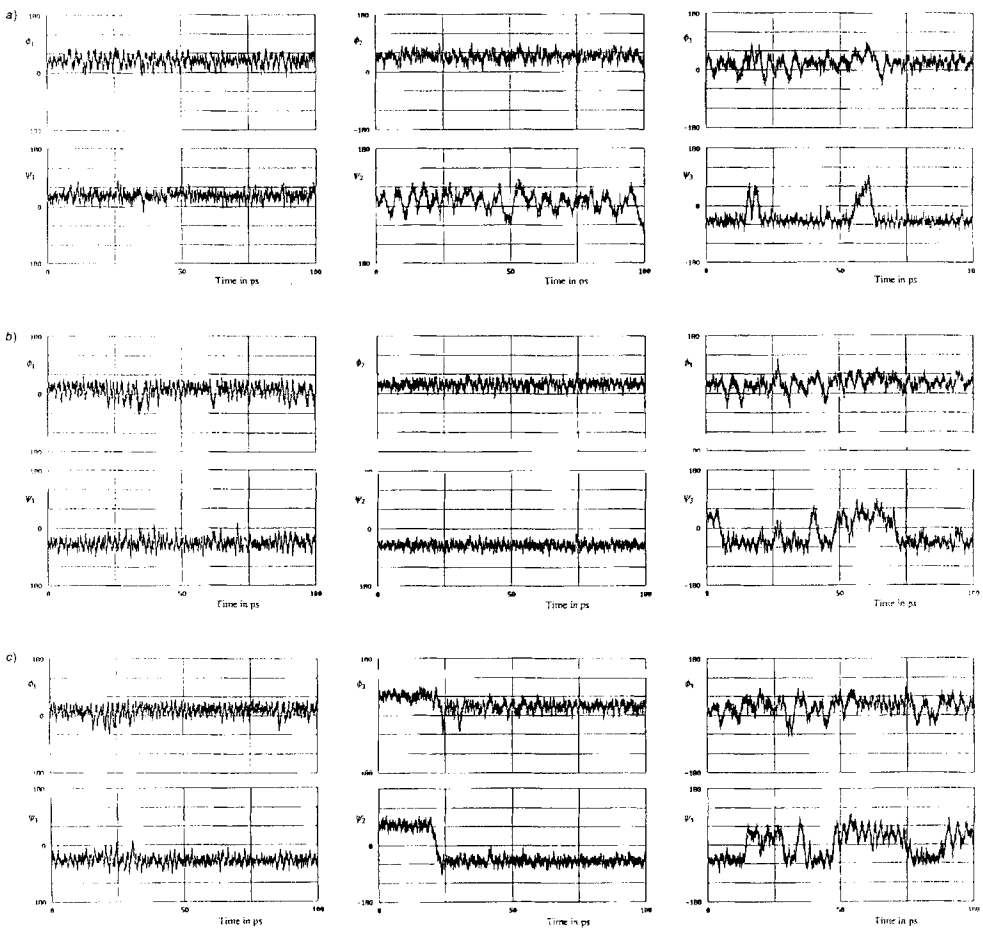

Fig. 6. *History of* ϕ_1, ψ_1, ϕ_2, ψ_2, ϕ_3, *and* ψ_3 *for the MD simulations starting from* a) **3AAB**, b) **3BBA**, *and* c) **3BCB** *over the entire trajectory, including equilibration*

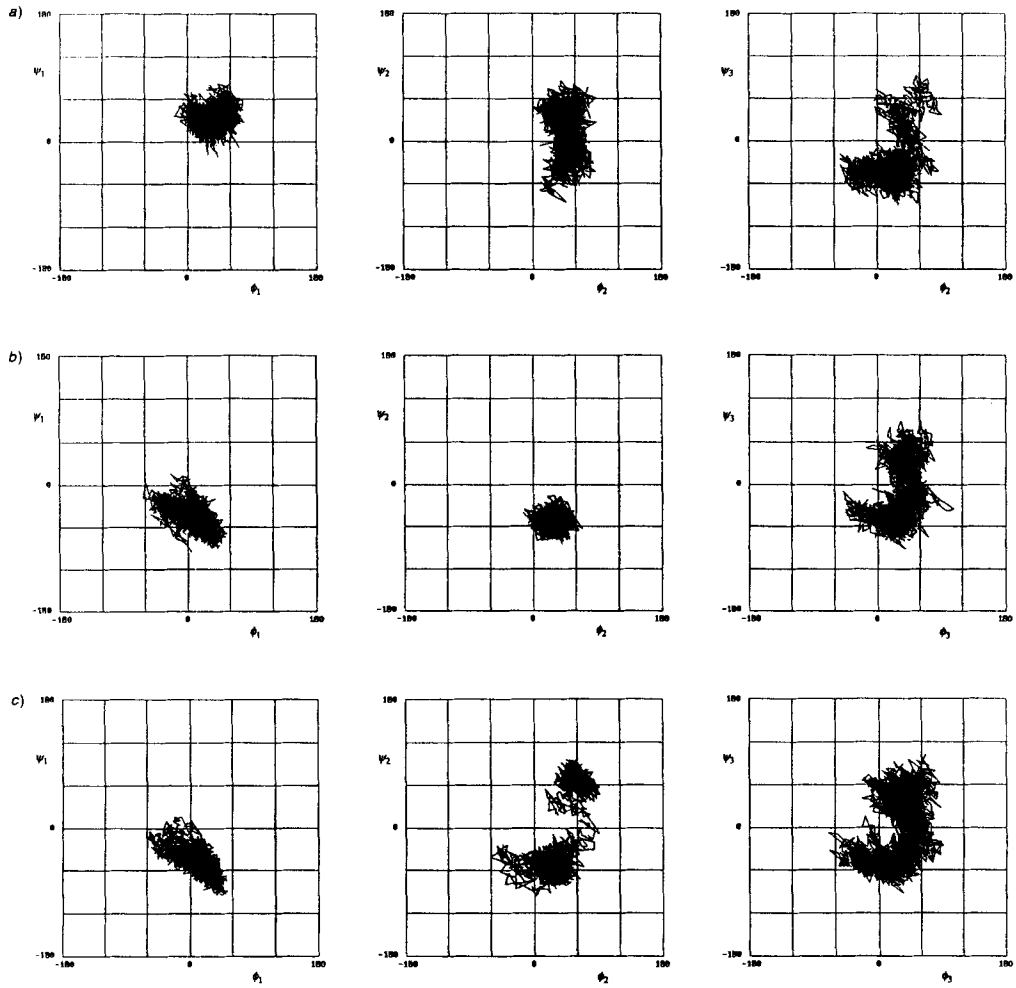

Fig. 7. *Trajectories on the* ϕ_1/ψ_1, ϕ_2/ψ_2, *and* ϕ_3/ψ_3 *maps for the MD simulations starting from* a) **3AAB**, b) **3BBA**, *and* c) **3BCB**, *including equilibration*

contrary some true transitions from the **B** to the **A** region (and *vice versa*) are observed at the GalNAc-Gal (*c-d*) glycosidic linkage. In short, during the simulation starting from **3AAB**, the molecule visits the conformers **3AAA** and **3AAB**, and also the conformer **3ACB** which is separated by a very low barrier from the latter.

As illustrated by *Fig. 6b* in the simulation starting from the conformer **3BBA**, only the third glycosidic linkage is flexible, and the molecule visits also the conformers **3BBB** and **3BBC**.

The simulation starting from the conformer **3BCB** can be divided in two periods: the first 20 ps (corresponding to the pre-equilibration period) and the other 80 ps. In the first period, the molecule visits the conformers **3BCB** and **3BCA**, but an irreversible transition

occurs after 20 ps (see the ϕ_2/ψ_2 trajectories) which moves the molecule to the **3BBA/3BBB/3BBC** portion of the conformational space with no back transition.

The eight conformers of compound **3** reported in *Table 1* can be distributed among three groups distinguishable through their dynamic behavior: *i*) **3AAB/3AAA/3ACB**, *ii*) **3BBA/3BBB/3BBC**, and *iii*) **3BCB/3BCA**, the third group being dynamically unstable. So, the calculations predict two groups of accessible conformations for **3**, and the dynamically averaged geometrical features of these two groups are to be compared with the NMR data as well as the geometrical features of the conformer **3BCB**.

The ROESY results of **3** (*Table 3*) are in close agreement with the distances calculated in the simulation from **3AAB** and in contrast with those calculated in the simulation from **3BBA** and for the conformer **3BCB**. In fact, the high H–C(5‴)/H–C(2′) cross-peak accompanied by the small CH_3(6‴)/H–C(2′) and H–C(3‴)/Ac cross-peaks are diagnostic of a precise orientation of the fucose residue with respect to the *N*-acetylgalactosamine residue *c*. The terminal trisaccharide portion *a*-*b*-*c* of **3** assumes exactly the same orientation as in **1** [3], *i.e.*, the residue *d* has no influence on the orientation of the other three. Thus, also in **3**, as in **1**, the *a*-*b* and the *b*-*c* glycosidic linkages present a low flexibility. On the contrary, the *c*-*d* glycosidic linkage exhibits a high flexibility as neither the **3AAB** conformer alone nor the **3AAA** conformer alone can account for the low intensity of the H–C(1′)/H–C(4) cross-peak. In the former conformer, a higher intensity should be observed, in the latter one, this cross-peak should not be observed.

It can be concluded that the conformational study here presented suggests that the tetrasaccharide **3** can be described by conformers **3AAB/3AAA** (and to a limited extent **3ACB**) and exhibits a low flexibility at the Fuc-Gal and Gal-GalNAc glycosidic linkages and a high flexibility at the GalNac-Gal one. Comparison of this behavior with that of the overlapping di- and trisaccharide sequences indicate that the rigidity of the trisaccharidic nonreducing terminus is dictated by the presence of the fucose residue as trisaccharide **7**, which lacks the residue *a*, has a high flexibility at both its glycosidic linkages. The *c*-*d* glycosidic linkage remains flexible in all the saccharides under study suggesting that the fucose moiety *a* does not extend its influence on the residue *d*. The β-D-GalNAc-(1→3)-α-D-Gal (*c*-*d*) sequence is also a fragment component of other relevant glycolipids, *e.g.* globoside and the *Forssman* antigen; both in the former [6] [7] and in the latter [8] case, a large flexibility was inferred around the ψ angle through modeling studies; this disaccharide maintains its flexibility also in our case though inserted in a different oligosaccharide chain.

Our results indicate that the residue *d* has no influence on the conformational behavior of the remaining *a*-*b*-*c* portion of **3**. The fact that its presence enhances the affinity towards the MBr1 antibody by about seven times might be due to some specific interaction of the residue itself with the active site of the antibody. In this respect, the epitope of the antigen **2** should include also the α-D-Gal residue of the saccharide moiety.

We acknowledge financial support provided by the Italian *Ministero dell'Università e della Ricerca Scientifica e Tecnologica*, Roma, and *Consiglio Nazionale delle Ricerche*, Roma. Contribution by Dr. *Pierangela Ciuffreda*, which assisted us in the NMR experiments, is also gratefully acknowledged.

Experimental Part

Compounds **3**, **6**, *and* **7**. The syntheses of propyl 3-*O*-{2-acetamido-2-deoxy-3-*O*-[2-*O*-(α-L-fucopyranosyl)-β-D-galactopyranosyl]-β-D-galactopyranosyl}-α-D-galactopyranoside (**3**) and of propyl 3-*O*-[2-acetamido-2-deoxy-3-*O*-(β-D-galactopyranosyl)-β-D-galactopyranosyl]-α-D-galactopyranoside (**7**) were described in [1]. The synthesis of propyl 3-*O*-(2-acetamido-2-deoxy-β-D-galactopyranosyl)-α-D-galactopyranoside (**6**) was described in [9].

^{1}H-NMR Experiments. Compounds **3**, **6**, and **7** were exchanged and lyophilized twice in 99.8% D_2O (*Merck*) and dried under high vacuum before dissolving in 99.96% D_2O (*Aldrich*) under N_2 (0.04M solns.). ^{1}H-NMR Spectra: at 303 K; *Bruker-AM500* spectrometer equipped with an *Aspect-3000* computer, a process controller, and an array processor; assignments by a combination of 1D and 2D COSY [10], TOCSY [11], and ROESY [12] experiments. TOCSY Spectra: MLEV-17 phase scheme [11], total mixing time 180 ms; 512 TPPI experiments, 32 transients per t_1, relaxation delay of 1.5 s; data were transformed as 2 $K \times 1$ K matrix. ROESY Spectra: phase-sensitive mode, pulse sequence 90-t_1-SL-FID where SL stands for a continuous spin-lock pulse of 200 ms at a field strength corresponding to a 90-deg pulse width between 80 and 90 μs; carrier frequency placed at the left side of the spectrum at 6.2 ppm to minimize *Hartmann-Hahn* effects [12]; spectral width 6024 Hz; 512 t_1 increments (32 scans each), spectral size in the time domain 2 K; zero filling to 1 K in the t_1 dimension before *Fourier* transformation. All 2D spectra were weighted with the squared sine-bell function shifted by $\pi/2$ in both dimensions. A NOESY spectrum of compound **3** was recorded in the TPPI mode using the pulse sequence described in [13]; however, it was not possible to observe NOESY cross-peaks due to the fact that, under these conditions, probably $\omega\tau_c \approx 1$.

MM and MD Calculations. Molecular-mechanics energy minimizations and molecular-dynamics simulations were performed with the HyperChem™ software from *Hypercube, Inc*. The MD simulations started from the optimized structures obtained by minimizations; the molecules were allowed to equilibrate at 300 K for a period of 20 ps followed by a period of 80 ps of data collection. A time step of 1 fs was used in the integration algorithm, and the trajectories were saved every 10 fs for further analysis. The H/H distances reported in *Table 3* were averaged over the period of data collection as $r = [\langle r^{-3} \rangle]^{-1/3}$ [5] as used for fast conformational changes. The glycosidic angles of compounds **3**, **6**, **7** were defined as ϕ_1 H–C(1‴)–O–C(2″), ψ_1 C(1‴)–O–C(2″)–H, ϕ_2 H–C(1″)–O–C(3′), ψ_2 C(1″)–O–C(3′)–H, ϕ_3 H–C(1′)–O–C(3), ψ_3 C(1′)–O–C(3)–H.

REFERENCES

[1] L. Lay, L. Panza, G. Russo, D. Colombo, F. Ronchetti, E. Adohati, S. Canevari, *Helv. Chim. Acta* **1995**, *78*, 533.
[2] L. Lay, F. Nicotra, L. Panza, G. Russo, E. Adobati, *Helv. Chim. Acta* **1994**, *77*, 509.
[3] L. Toma, P. Ciuffreda, D. Colombo, F. Ronchetti, L. Lay, L. Panza, *Helv. Chim. Acta* **1994**, *77*, 668.
[4] E.G. Bremer, S.B. Levery, S. Sonnino, R. Ghidoni, S. Canevari, R. Kannagi, S. Hakomori, *J. Biol. Chem.* **1984**, *259*, 14773.
[5] J. Tropp, *J. Chem. Phys.* **1980**, *72*, 6035.
[6] J.N. Scardsale, R.K. Yu, J.H. Prestegard, *J. Am. Chem. Soc.* **1986**, *108*, 6778.
[7] L. Poppe, C.-W. von der Lieth, J. Dabrowski, *J. Am. Chem. Soc.* **1990**, *112*, 7762.
[8] G. Grönberg, U. Nilsson, K. Bock, G. Magnusson, *Carbohydr. Res.* **1994**, *257*, 35.
[9] D. Colombo, L. Panza, F. Ronchetti, submitted to *Carbohydr. Res.*
[10] K. Nagayama, A. Kumar, K. Wuetrich, R.R. Ernst, *J. Magn. Reson.* **1980**, *40*, 321.
[11] A. Bax, D.G. Davis, *J. Magn. Reson.* **1985**, *63*, 355.
[12] A. Bax, D.G. Davis, *J. Magn. Reson.* **1985**, *63*, 207.
[13] G. Bodenhausen, H. Kogler, R.R. Ernst, *J. Magn. Reson.* **1984**, *58*, 370.